Electronic and optical properties of fluorine-doped tin oxide films

A. E. Rakhshani,[a] Y. Makdisi, and H. A. Ramazaniyan
Physics Department, Kuwait University, PO Box 5969, Safat 13060, Kuwait

(Received 26 March 1997; accepted for publication 7 October 1997)

Thin films of fluorine-doped SnO_2 have been prepared by deposition on borosilicate glass using the spray-pyrolysis technique. The effect of doping on the concentration and mobility of the charge carriers (electrons) as well as the resistivity of the films has been studied. The undoped films had a resistivity of a few m Ω cm; this could be reduced by a factor of 10 by doping. The electron mobility in undoped films was about 3 cm^2/Vs but could be improved by a factor of 5 to 6 by doping. The doping yield was about 2.3%. The high quality films which were deposited for photovoltaic applications had a sheet resistance of $R_\square = 2\ \Omega/\text{sq}$ and an average transmittance, in the visible region, of $T = 85\%$ for a thickness of 1.1 μm. Their figure of merit is one of the highest values reported: $\phi = T^{10}/R_\square \approx 0.1$ S. The optical dispersion of our films can be explained perfectly by classical models. In the wavelength region of $\lambda < 0.580\ \mu$m, the refractive index, N, for undoped and doped films can be given by $N = [1 + \lambda^2/(0.370\lambda^2 - 0.0105)]^{1/2}$, where λ is in μm. From the study of dispersion and the plasma resonance frequency, the numerical values at optical frequencies of the dielectric constant, electron mobility, and electron effective mass were determined as 3.70, 9.3–11.8 cm^2/Vs, and $(0.26–0.45)m_0$, respectively, where m_0 is the mass of free electrons. From the variation of direct and indirect optical transition energies with the carrier concentration, the density-of-states effective masses for electrons and holes were obtained as $0.85\ m_0$ and $0.78\ m_0$, respectively. These studies revealed a direct energy bandgap of 4.11 eV for SnO_2 in addition to a defect band situated 0.45 eV above the valence band edge. © *1998 American Institute of Physics.* [S0021-8979(98)02502-X]

I. INTRODUCTION

Tin oxide is a wide bandgap nonstoichiometric semiconductor with a low n-type resistivity ($\approx 10^{-3}\ \Omega$cm) and high transparency ($\approx 90\%$) in the visible region. The nonstoichiometric resistivity can be reduced further to the range of $10^{-4}\ \Omega$ cm by doping, a level suitable for application in thin film solar cells.[1,2] In addition to solar cell technology, tin oxide has also been used in fabrication of gas sensors due to the sensitivity of its surface conductance to gas adsorption.[3,4] Other applications, preparation techniques, and properties of tin oxide have been reviewed.[5]

Fabrication techniques used to deposit tin oxide include dip coating, evaporation, sputtering, chemical vapor deposition, and spray pyrolysis. This paper reports on films made by spray pyrolysis which is a method of producing large area high-quality low-cost films. The tin compounds used in spray pyrolysis solutions have mainly been $SnCl_2$ (Ref. 6) and $SnCl_4$ (Ref. 7). Recently, the use of SnF_2 has also been reported.[8] Doping with Sb,[9,10] Cl,[7,11] Br,[7] and F[7,12–15] has been achieved by adding a suitable compound of the dopant to the spray solution. Fluorine has been shown to be the most effective of these dopants.[7]

Work on fluorine-doped tin oxide (SnO_2:F) has resulted in data on the electrical and optical properties which displays some scatter (as for other dopants). The variation in the reported data could be the result of the different recipes used for the spray solutions (given in Table I). The ratio of the molar concentration of oxygen and tin varies from solution to solution and is much greater than 2 in all solutions except in solution 6. Solution 6, which has resulted in high-quality films with a transmittance of $\approx 90\%$ and a sheet resistance of 12 Ω/sq for 0.5 μm thick films (resistivity $\approx 5 \times 10^{-4}\ \Omega$ cm),[13] seems to have the better composition; however, details of the optical and electrical properties of the films obtained with this solution were not discussed. The aim of this work was to characterize films of this quality reproduced in our laboratory for use in electrodeposition of CdTe and the fabrication of photovoltaic cells. The optical characterization of these films (including dispersion and optical transitions) is also reported here.

II. MEASUREMENTS AND EVALUATION METHODS

A. Sample preparation and measurements

SnO_2:F films were deposited from a solution comprising 23 ml of $SnCl_4$, 7 ml of H_2O, and 920 ml of methanol (solution 6, Table I). Fluorine was added in the form of HF, instead of NH_4F,[13] to give the solution a doping level of F/Sn in the range of 0–180 atomic percent (at. %). Deposition was performed on borosilicate glass substrates at a temperature of 490 °C–525 °C and from a distance of approximately 18 cm using a spray bottle with a nozzle diameter of 0.5 mm. The carrier gas was nitrogen and the spray rate was ≈ 12 ml/min. The spray bottle had a design similar to that for the Thomas Scientific model 2753-10.

Initial estimates of the thickness of films was obtained from the mass of the deposit using a density of 6.99 g/cm^3.[16] Thickness estimates from the mass deposited and its density is a convenient and proven method which has been applied to many thin solid films including Cu_2O[17,18] and CdTe.[19] In SnO_2:F films, the possible change of density with heavy

[a]Corresponding author.

TABLE I. The molar concentration of tin, oxygen, and their ratio in the $SnCl_4$-based spray solutions. Sources of oxygen are H_2O in the solution, air in the carrier gas, or air in the ambient. Solutions 1, 2, 3, and 5 contain an additional amount of HCl.

No.	Solvent	Sn	O	O/Sn	Oxygen source	Dopant	Reference
1	propanol	0.37	23	62	water	Sb	10
2	propanol	0.53	⋯	⋯	air	Sb	9
3	ethanol	1.37	24.6	18	water	Cl	11
4	methanol	0.17	5.5	32	water & air	Br, Cl, F	7
5	ethanol	2.5	20.5	85	water	F	12
6	methanol	0.2	0.4	2	water	F	13
7	ethanol	0.6	⋯	⋯	air	F	14
8	butyl acetate	2.5	⋯	⋯	air(ambient)	F	15

doping is negligible since the crystal structure remains the same and the atomic mass of oxygen and fluorine are close to each other. The thicknesses calculated from interference patterns in the transmittance or reflectance spectra of the films using the refractive index of 2.0 reported for SnO_2 at 589.3 nm[16] were in good agreement with our initial estimates.

After the dispersion equation for SnO_2 was established experimentally (Sec. III B), the routine thickness measurement was performed using the interference patterns. The optical transmittance and reflectance spectra were measured in the wavelength range of 200–3300 nm with a Cary-5E double-beam spectrophotometer.

The sheet resistance and Hall coefficient were measured by the four-point-probe and the Van der Pauw's techniques, respectively.

B. Evaluation of optical properties

In this section, the methods and the theoretical models used for the characterization of samples are discussed in brief.

In the interference-free region of the spectrum, the transmittance, T, of an absorbing film on a transparent substrate, taking into account the multiple incoherent reflections at interfaces, can be written as[20,21]

$$T=\frac{Me^{-\alpha d}}{P-Qe^{-2\alpha d}}. \tag{1}$$

Above, d is the film thickness, α its absorption coefficient, $M=(1-R_1)(1-R_2)(1-R_3)$, $P=(1-R_2R_3)$, and $Q=R_1R_2+R_1R_3-2R_1R_2R_3$ in which R_1, R_2, and R_3 are the reflection coefficients of the air film, film substrate, and substrate-air interfaces, respectively:

$$R_1=\frac{(N-1)^2+k^2}{(N+1)^2+k^2}, \quad R_2=\frac{(N-N_S)^2+k^2}{(N+N_S)^2+k^2},$$

$$R_3=\frac{(N_S-1)^2}{(N_S+1)^2},$$

where N and $k=\lambda\alpha/4\pi$ are the refractive index and the extinction coefficient of the film and N_s is the refractive index of the glass substrate (λ is the wavelength of the incident beam). To determine α, transmittance measurements were performed in the wavelength range of 260–320 nm with a plain glass substrate in the reference-beam compartment of the spectrometer. Since this compensates for absorption in the substrate, one may set $M=(1-R_1)(1-R_2)$. Also, in this range of wavelengths, $\alpha d \gg 1$ and Eq. (1) can be simplified to

$$T=Ae^{-\alpha d}, \tag{2}$$

where $A=(1-R_1)(1-R_2)/(1-R_2R_3)$. Equations (1) and (2) have been used in the characterization of other thin films and have yielded reliable data.[17–19]

For SnO_2, k decreases from ≈ 0.2 at $\lambda=266$ nm to ≈ 0.02 at $\lambda=310$ nm. The variation of N is much weaker: $N=2.0$ at 589.3 nm;[16] interference patterns in reflectance and transmittance spectra imply that, at 290 nm (the middle of the wavelength range of interest), $N=2.25$ (see below). Using $N=2.25$ and an average value of 0.1 for k, $A=0.816$. It turns out that the error in the calculation of α due to neglect of the variation in N in the wavelength range of interest is less than 5%.

The interference pattern superimposed on a transmittance or reflectance spectrum was used to determine the film's refractive index at wavelengths corresponding to peaks and valleys. If λ_j is the wavelength at which the peak or valley of order j occurs, then

$$4d\beta\, N(\lambda_j)=j\lambda_j \quad (j=1,2,3,...). \tag{3}$$

In reflectance measurements the incident angle of the beam was $\theta_i=20°$. This implies $\beta\equiv[1-\sin^2\theta_i/N^2(\lambda_j)]^{1/2}\approx 1-0.058/N^2(\lambda_j)$ so that the change in β as N varies in the vicinity of 2 is negligible; for $N=2$, $\beta=0.985$. In transmittance measurements, $\theta_i=0°$ and $\beta=1$. The evaluation of N by this method does not require the measurement of absolute values of transmittance or reflectance. In practice, its accuracy is limited only by the accuracy to which the thickness d (which must be measured independently) is known.

It is possible to evaluate simultaneously both N and d from absolute values of transmittance by the Swanepoel method[21] if scattering of incident beam by the film is negligible, (not taken into account in this method). The method is useful particularly for amorphous layers or polycrystalline films with small grain sizes. The accuracy of estimating d from the mass deposited was checked by applying the Swanepoel method to the transmittance data of a thin sample which has very small grains (Fig. 2, undoped sample). The measured value for d was 0.297 μm compared to the mass-based estimate of 0.28 μm. The 7% difference can be taken as a measure of the accuracy of thickness estimates from

mass deposits. To extend the interference patterns to long wavelengths, all samples used for measurement of dispersion had to be relatively thick (about 1 μm) and consequently grains were quite large (fraction of 1 μm) and therefore scattering could not be ignored. Application of the Swanepoel method to these films lead to erroneous results and therefore Eq. (3) was used for the evaluation of the refractive index of films.

For a range of wavelengths corresponding to subbandgap energies (where $k \ll N^2-1$), the dispersion relation (classical) for bound electrons (BE) applies,[22]

$$\frac{1}{N^2-1}=\frac{\lambda_0^2}{\varepsilon_\infty-1}\left(\frac{1}{\lambda_0^2}-\frac{1}{\lambda^2}\right) \quad (\lambda>\lambda_0), \tag{4a}$$

$$\varepsilon_\infty=1+\frac{e^2 n_{\mathrm{BE}}\lambda_0^2}{4\pi^2 c^2 \varepsilon_0 m_{\mathrm{BE}}}. \tag{4b}$$

Above, λ_0 is a characteristic wavelength associated with the resonance frequency of the bound electrons and ε_∞ is the nondispersive optical dielectric constant. m_{BE} and n_{BE} denote the effective mass and concentration of bound electrons, respectively, c is the speed of light, ε_0 the permittivity of free space, and e the electronic charge. From a fit of the experimental results on dispersion to Eq. (4a), one can determine the values of λ_0 and ε_∞, and, therefore, $n_{\mathrm{BE}}/m_{\mathrm{BE}}$.

When the dispersion due to free electrons (FE) becomes dominant at longer wavelengths (still $k^2 \ll N^2$) the dispersion equation is given by[22]

$$N^2=\varepsilon_\infty+\chi-\frac{e^2 n}{\varepsilon_0 m_n\left(\dfrac{4\pi^2c^2}{\lambda^2}+g^2\right)}. \tag{5}$$

Here, n is the concentration of free electrons, m_n is their effective mass, χ represents the contribution from other processes such as interband electronic transitions,[23,24] and $g=e/m_n\mu_\infty$, where μ_∞ is the mobility of free electrons at the optical frequencies involved. For $\mu_\infty \approx 10\ \mathrm{cm^2/Vs}$ and $m_n \approx 0.5\, m_0$ (typical values for SnO_2, see Sec. III), the g^2 term becomes negligible with respect to the term $4\pi^2c^2/\lambda^2$ for wavelengths shorter than $\approx 2\ \mu$m and Eq. (5) reduces to

$$N^2=\varepsilon_\infty+\chi-\frac{e^2 n}{4\pi^2 c^2 \varepsilon_0 m_n}\lambda^2. \tag{6}$$

A fit to dispersion data for these wavelengths [using Eq. (6)], allows one to fix m_n and χ.

In the FE dispersion region, the reflectance R and the plasma resonance frequency, $\omega_p=2\pi c/\lambda_m$, both increase with increasing n (λ_m is the wavelength corresponding to the minimum reflectivity). Since minimum reflectivity corresponds to $N=1$, the following expression (first obtained by Drude[25]) can be derived from Eq. (5):

$$\omega_p^2=\frac{e^2 n}{\varepsilon_0(\varepsilon_\infty+\chi-1)m_n}-g^2. \tag{7}$$

By measuring ω_p for several samples with different doping levels and fitting the results to Eq. (7), one can determine the value of g and consequently μ_∞.

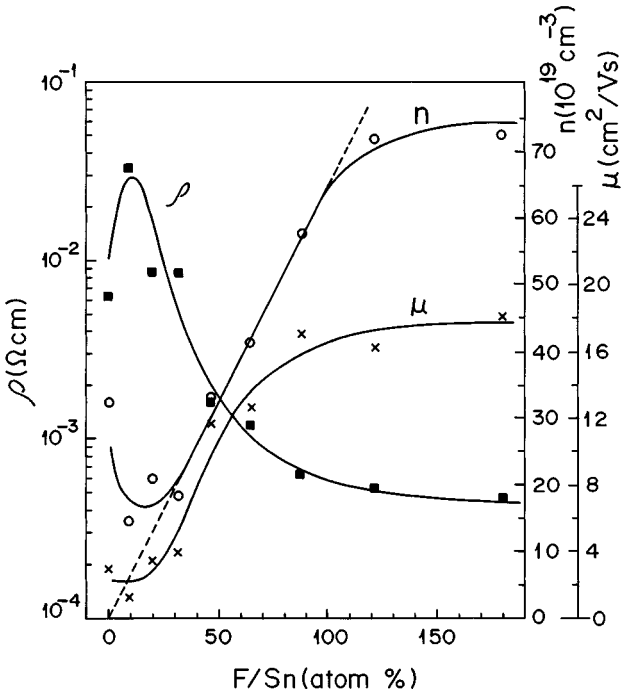

FIG. 1. Variation of film's resistivity (ρ), electron concentration (n), and electron mobility (μ) with the doping level in spraying solution.

In the determination of direct and indirect optical transitions from absorption coefficient data, the general procedure is to fit the data to theoretical models. The variation of an absorption coefficient with photon energy, E, in the case of a direct-allowed transition is[26]

$$\alpha=A(E-E_d)^{1/2} \quad (E>E_d), \tag{8}$$

where E_d is the direct-allowed transition energy. For indirect-allowed transitions

$$\alpha=B\left(\frac{(E-E_i+E_p)^2}{\exp(E_p/\mathrm{kT})-1}+\frac{(E-E_i-E_p)^2}{1-\exp(-E_p/\mathrm{kT})}\right), \tag{9}$$

where the transition is assisted by absorption (first term in bracket) or emission (second term) of a phonon of energy E_p. In the use of Eq. (9), it is essential that the second term be taken as zero for $E<E_i+E_p$. The proportionality factors A and B are treated as energy independent constants by some authors, who then use plots of α^2 or $\alpha^{1/2}$ against E to identify the type of transition and derive E_d, E_i, and E_p. A and B, however, are inversely proportional to E through their dependence on oscillator strength for the transition.[22] Consequently, we have chosen to plot $(\alpha E)^2$ and $(\alpha E)^{1/2}$ vs E. In both cases straight lines resulted but the transition energies implied are slightly different.

III. EXPERIMENTAL RESULTS AND DISCUSSION

A. Doping effect

Films with a thickness in the range of 0.25–0.30 μm were deposited from solutions with different concentration of dopant. Figure 1 shows the variation in electrical resistivity (ρ), electron (majority carrier) concentration (n), and electron mobility (μ) with the solution doping level. As the dop-

ing level increases, the resistivity increases initially due to a decrease in n, and then decreases monotonically to $\approx 5 \times 10^{-4}\ \Omega$ cm for F/Sn values greater than ≈ 130 at. %. The initial decrease in n at F/Sn$\approx$13 at. % corresponds to a lower concentration of oxygen vacancies as the result of fluorine incorporation. Although the O/Sn atomic ratio in the solution was 2, apparently not all oxygen atoms participate in forming SnO_2, especially with the reducing effect of methanol which decomposes to CO and H_2 during deposition. The oxygen deficiency occurs also in films prepared from solutions with much higher O/Sn atomic ratios as listed in Table I, possibly due to the effect of methanol.[7] After the initial decrease in n, the electron concentration increases almost linearly with fluorine concentration up to F/Sn$\approx$90 at. % and then saturates at $n \approx 7.5 \times 10^{20}\ \mathrm{cm}^{-3}$. SnO_2 has a tetragonal crystal lattice ($a = 0.474\ \mathrm{nm} = b$, $c = 0.319\ \mathrm{nm}$[27]) and a density of $6.99\ \mathrm{g/cm}^3$.[16] From these data, it is concluded that there must be two molecules per unit cell and the number of molecules per $1\ \mathrm{cm}^3$ of SnO_2 is $n_0 = 2.8 \times 10^{22}$. The doping yield, defined as the ratio of n/n_0 over F/Sn, is 0.023 in the linear range of doping shown in Fig. 1. This implies that only 2.3% of sprayed fluorine atoms become active donors; the rest either do not enter the lattice or get incorporated inactively in the grain boundaries.[28] The latter mechanism is more likely, since it can explain the variation of mobility with doping. As shown in Fig. 1, doping with F has a significant effect on the Hall mobility of electrons. The mobility increases with the F/Sn ratio and saturates at about $18\ \mathrm{cm}^2/\mathrm{Vs}$. The mobility in undoped samples was as low as $\approx 3\ \mathrm{cm}^2/\mathrm{Vs}$ compared to a value of $90\ \mathrm{cm}^2/\mathrm{Vs}$ reported for a single crystal of SnO_2.[29,30] The low mobility in undoped samples could be due to the scattering of electrons from grain boundaries as well as oxygen-vacancy defects. The effect of oxygen-vacancy scattering is seen by comparing the value of $3\ \mathrm{cm}^2/\mathrm{Vs}$ measured in our sample with the higher value of $14\ \mathrm{cm}^2/\mathrm{Vs}$ reported for samples with less oxygen deficiency (air as the carrier gas and O/Sn=32 at. %).[7] These latter samples have, as one would expect, a lower carrier concentration of $\approx 12 \times 10^{19}\ \mathrm{cm}^{-3}$ in comparison to $\approx 32 \times 10^{19}\ \mathrm{cm}^{-3}$ of our sample. The increase of mobility with doping concentration beyond F/Sn$\approx$26 at. %, where the effect of oxygen-vacancy scattering has already been reduced by fluorine incorporation in vacancies,[31] is most probably due to the effect of fluorine in reducing the grain-boundary-related activation energy of mobility.[9] The variation of mobility with doping shown in Fig. 1 is different from that for samples with less oxygen deficiency.[7] In the latter case, μ decreases when the F/Sn ratio exceeds ≈ 15 at. %.

The electrical properties of our samples when highly doped are in excellent agreement with the values of $n = 6.9 \times 10^{20}\ \mathrm{cm}^{-3}$, $\mu = 17.5\ \mathrm{cm}^2/\mathrm{Vs}$ and $\rho = 5.15 \times 10^{-4}\ \Omega$ cm reported for the fluorine-doped films deposited by chemical vapor deposition (CVD) technique.[32] For undoped films produced by the CVD technique, $n = 22 \times 10^{19}\ \mathrm{cm}^{-3}$, $\mu = 8.5\ \mathrm{cm}^2/\mathrm{Vs}$, and $\rho = 33 \times 10^{-4}\ \Omega$ cm, which, except for the mobility, are also comparable with the data shown in Fig. 1.

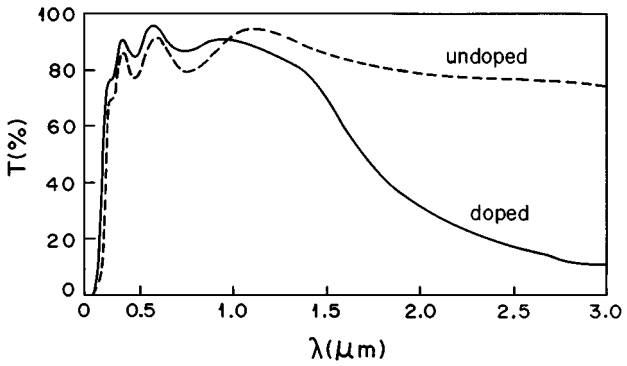

FIG. 2. The transmittance T against wavelength λ for undoped and heavily doped films. For the undoped film $n = 3.2 \times 10^{20}\ \mathrm{cm}^{-3}$, $\rho = 63.4 \times 10^{-4}\ \Omega$cm, and thickness is $d = 0.28\ \mu$m. For the doped film $n = 7.2 \times 10^{20}\ \mathrm{cm}^{-3}$, $\rho = 4.7 \times 10^{-4}\ \Omega$ cm, and $d = 0.25\ \mu$m.

B. Optical properties and dispersion

Figure 2 contains the optical transmittance spectra of the first (undoped) and the last (heavily doped) sample in the series of samples on which Fig. 1 is based. The average transmittance in the visible region is about 90% for the doped film which has a sheet resistance of 19 Ω/sq. The doped film has a higher transmittance at short wavelengths than the undoped film. This is not because its thickness is slightly smaller. It is mainly due to the effect of doping which improves the transparency as the result of shifting the direct optical transition towards shorter wavelengths. This effect will be discussed in detail in Sec. III C. The decrease in the transmittance of doped film in the near-infrared region indicates an increase in reflectance due to conduction electrons.

Haacke's figure of merit[33] for the photovoltaic application of transparent conducting films is defined as $\phi = T^{10}/R_{\square}$, where T and $R_{\square}$ are the transmittance and the sheet resistance, respectively. This figure of merit and other relevant parameters for three highly-doped samples are given in Table II. Sample 1 is the doped sample whose transmittance is shown in Fig. 2. Although it has a high transmittance, its high sheet resistance has reduced its figure of merit. Sample 2, with an intermediate thickness of 0.41 μm, has a much better value of $\phi = 38.7 \times 10^{-3}$ S. Sample 3, with a higher thickness of 1.1 μm, has an excellent value of $\phi = 98 \times 10^{-3}$ S; this figure of merit is almost twice that of commercial samples (Nippon Glass Co.)[8] and also greater than the highest value of $\phi = 71.2 \times 10^{-3}$ S reported for films prepared by CVD technique.[32]

The dispersion of SnO_2 films was determined from interference patterns in the reflectance spectra. Figure 3 shows the dispersion curves for an undoped and a fluorine-doped sample. This undoped sample is different from that of Fig. 2. The dashed line shows the expected curve in the absence of FE dispersion. The data for the two samples match in the short wavelength range, where BE dispersion is the dominant mechanism. The effect of FE dispersion in reducing N below the dashed line is more pronounced in the doped sample, which is to be expected because of its higher free electron concentration.

TABLE II. Figures of merit for SnO_2:F samples prepared in this work and reported by others. The electron concentration (n), resistivity (ρ), thickness (d), sheet resistance ($R_\square$), and transmittance (T) values are listed. T is the average transmittance in the visible region, except for the last two values which correspond to a wavelength of 650 nm.

Sample	$n(10^{20}\ \mathrm{cm}^{-3})$	$\rho(10^{-4}\ \Omega\ \mathrm{cm})$	$d(\mu\mathrm{m})$	$R_\square(\Omega)$	$T(\%)$	$\phi(10^{-3}\ S)$
1	7.2	4.7	0.25	19	90	18.3
2	8.8	3.7	0.41	9	90	38.7
3	7.6	2.2	1.1	2	85	98.4
Reference 32	7.1	5	0.65	7.5	94	71.2
Reference 8	⋯	⋯	⋯	5.6	85	35.3
Reference 8	(Nippon Glass Co.)	⋯	⋯	6	89.1	52.5

In the nondispersive range of wavelengths, where $\lambda \gg \lambda_0$, N^2 becomes constant and equal to the nondispersive optical dielectric constant ϵ_∞. Figure 4 shows the perfect fit of the experimental data of Fig. 3 to Eq. (4a) in the wavelength region of 0.280–0.580 μm. As seen, the data for the doped and undoped samples match each other when BE dispersion becomes dominant. From the slope and the vertical intercept of the straight line, numerical values for λ_0 and ϵ_∞ of 0.169 μm and 3.70, respectively, were determined for both samples. These values and others which were obtained during this study are listed in Table III. Knowing $\epsilon_\infty = 3.70$, it is possible to express m_{BE} in terms of n_{BE} using Eq. (4b). Observe $n_{\mathrm{BE}} = n_0 f$, where n_0 is the number of SnO_2 molecules per unit volume ($n_0 = 2.8\times 10^{28}\ \mathrm{m}^{-3}$) and f denotes the number of bound electrons per SnO_2 molecule which contribute to BE dispersion. Thus, we find that $m_{\mathrm{BE}}/m_0 = 0.265f$, where m_0 is the free-electron mass. The value of m_{BE} implied by this result is in a reasonable range for $f = 1$ to almost 4 if m_{BE} is similar in magnitude to the effective mass of holes. Using the values for ϵ_∞ and λ_0 in the wavelength range of $0.280 < \lambda < 0.580\ \mu$m (in which N is independent of doping level), the dispersion formula can be written as:

$$N = \left[1 + \frac{\lambda^2}{0.370\lambda^2 - 0.0105}\right]^{1/2}, \tag{10}$$

where λ is in μm. The fit of this equation to the experimental data is shown by the dashed line in Fig. 3.

In degenerate semiconductors, where FE dispersion is dominant at much lower wavelengths than in nondegenerate semiconductors, the nondispersive part in n-λ plots disappears. Instead of approaching a constant value, N continues to decrease monotonically with increasing λ as shown in Fig. 3.

Figure 5 shows the perfect fit of the experimental data for the doped sample in the wavelength range of $\lambda \geqslant 0.58\ \mu$m to the FE dispersion formula, Eq. (6). The slope and the vertical intercept of the resulting straight line yield $m_n/m_0 = 0.45$ and $\chi = 0.66$. For the undoped sample in Fig. 5, and also for other undoped samples examined, the fit to

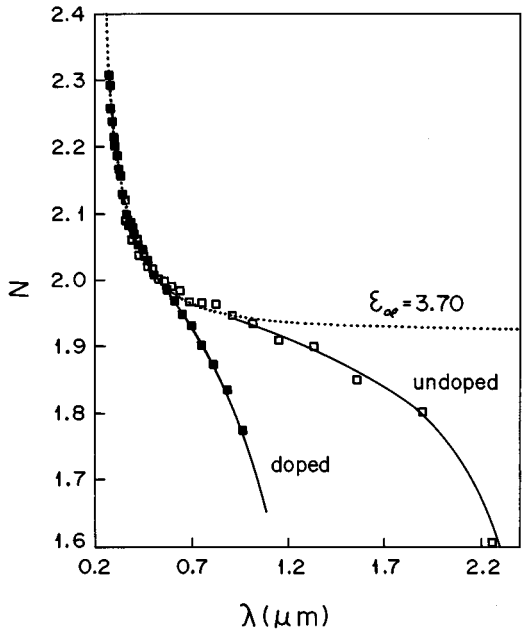

FIG. 3. The wavelength dependence of the refractive index, N, of an undoped ($n = 1.1\times 10^{20}\ \mathrm{cm}^{-3}$) and a F-doped ($n = 6.6\times 10^{20}\ \mathrm{cm}^{-3}$) sample of SnO_2. The dashed line shows the contribution of only bound electrons corresponding to an optical dielectric constant of $\varepsilon_\infty = 3.70$. The nondispersive value for the reflective index is $N_0 = \varepsilon_\infty^{1/2} = 1.924$.

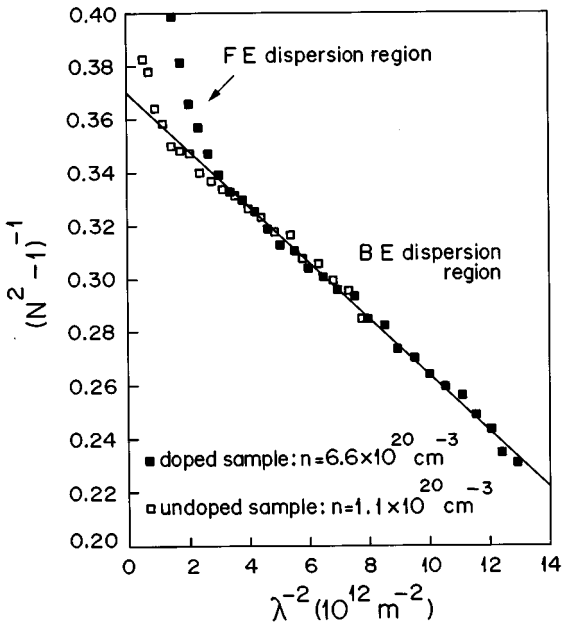

FIG. 4. The fit of the experimental data presented in Fig. 3 to the bound-electron dispersion formula, Eq. (4a). This fit yields $\lambda_0 = 0.169\ \mu$m, $\varepsilon_\infty = 3.70$, and $m_{\mathrm{BE}}/m_0 = 0.265f$.

TABLE III. Summary of the results obtained from the optical characterization of SnO_2:F films. The measured parameters are the characteristic wavelength (λ_0), optical dielectric constant (ϵ_∞), contribution to the dielectric constant from interband transitions (χ), hole effective mass (m_p), electron effective mass (m_n), electron mobility at optical frequencies (μ_∞), electron relaxation time (τ), phonon energy (E_p), indirect (E_i) and direct (E_d) transition energies, direct energy bandgap (E_g), and the energy of a defect band (Δ) measured from the valence band edge (m_0 is the free-electron mass).

Parameter	Dispersion	Plasma resonance frequency	Optical transitions
λ_0	0.169 μm		
ϵ_∞	3.70		
χ	0.66(0.30[a])		
$\frac{m_p}{m_0}$	$0.265f$[b]		0.78[c]
$\frac{m_n}{m_0}$	0.45(0.40[a])	0.26	0.85[c]
μ_∞		9.3–11.8(10.0[a]) cm^2/Vs	
τ		1.75×10^{-15} s	
E_p			20–50 meV
E_i			3.68–3.88 eV
E_d			4.16–4.54 eV
E_g			4.11 eV (direct)
Δ			0.45 eV

[a]Undoped sample.
[b]f is the number of bound electrons per SnO_2 molecule participating in dispersion.
[c]Density-of-states effective mass.

Eq. (6) was not satisfactory; instead, Eq. (5) had to be used. This is due to the fact that Eq. (6) is valid for $\lambda \ll 2\ \mu$m, as discussed before, whereas FE dispersion starts to become effective in undoped samples for $\lambda \geqslant 1\ \mu$m (see Figs. 3 or 4). The dashed line in Fig. 5 shows the dependence of N^2 on λ^2 according to Eq. (5) with $\epsilon_\infty = 3.70$, $m_n/m_0 = 0.40$, $\chi = 0.30$, and $\mu_\infty = 10\ cm^2/Vs$. The last three values were found to be the best combination for fitting this plot to the experimental data. For the undoped film, χ is almost half of that for the doped sample, indicating that the contribution from interband transitions to the dielectric constant increases with doping.

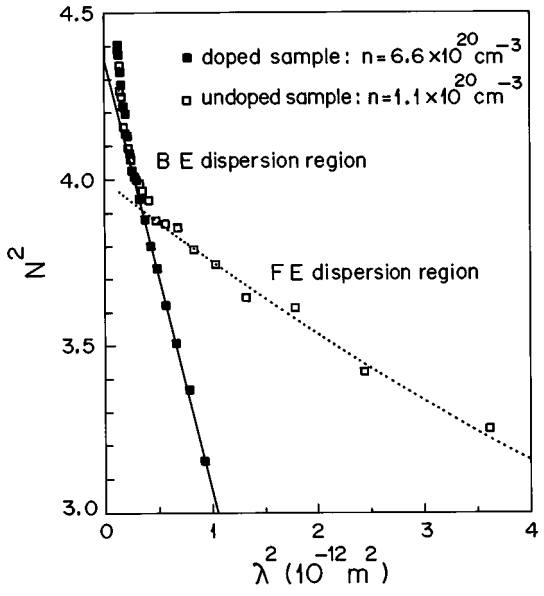

FIG. 5. The fit of the experimental data presented in Fig. 3 to the free-electron dispersion formula, Eq. (6). The fit for the doped sample implies $m_n/m_0 = 0.45$ and $\chi = 0.66$. The dashed line is the best fit of Eq. (5) to the data of undoped sample, taking $m_n/m_0 = 0.40$, $\chi = 0.30$, and $\mu_\infty = 10\ cm^2/Vs$.

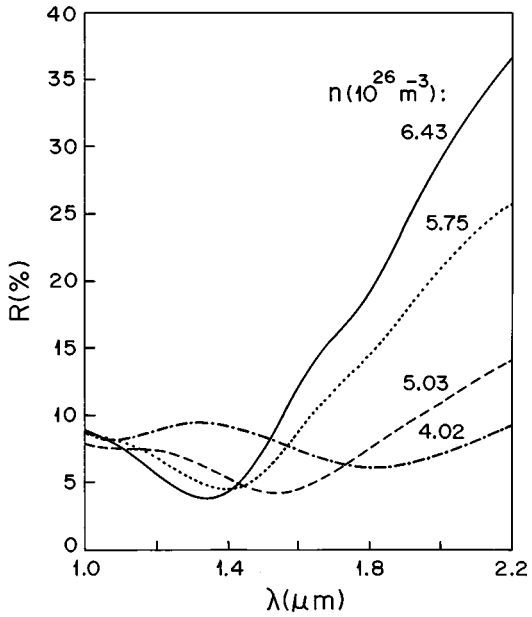

FIG. 6. Specular reflectance spectra of a few samples with different electron concentration, n.

The parameter g in Eq. (5) is, in general, wavelength dependent through its dependence on μ_∞. If charged-impurity scattering is the dominant mechanism, g varies as $\lambda^{3/2}$ for wavelengths smaller than the plasma resonance wavelength.[15,34] In our samples, however, the magnitude of g^2 remains much smaller than the $4\pi^2c^2/\lambda^2$ term in the measured range of wavelengths and therefore the dependence of g on λ cannot be inferred.

Figure 6 shows the spectrum of specular reflectance for a few samples with different doping levels. They have almost identical thicknesses in the range of 0.26–0.30 μm (determined from interference patterns). The fit of Eq. (7) to the experimental data extracted from Fig. 6 is shown in Fig. 7. Using the slope and the vertical intercept of this straight-line fit and taking $\chi = 0.66$ it is found that $m_n/m_0 = 0.26$ and $g = 5.7\times10^{14}\ s^{-1}$. Thus, $\mu_\infty = 11.8\ cm^2/Vs$ and the electron relaxation time $\tau = g^{-1} = 1.75\times10^{-15}$ s. The variation of χ with doping does not have a significant effect on the above values: Even if the effect of χ is neglected (we set $\chi = 0$), the value of m_n/m_0 increases only to 0.33 with a corresponding decrease in μ_∞ to $9.3\ cm^2/Vs$. The value of 0.26–0.33 for m_n/m_0 is not too far below the value of 0.45 obtained from Fig. 5. Equation (7), but without the g^2 and χ terms, implies the value $m_n/m_0 = 0.35$ for identical samples ($n = 6.9\times10^{20}\ cm^{-3}$ and $\mu = 17.5\ cm^2/Vs$) prepared by CVD technique.[32]

The linear dependence of ω_p^2 on n, as demonstrated in Fig. 7 indicates that m_n is constant and independent of the doping level. This implies that the curvature of conduction band in momentum space does not change with doping level.

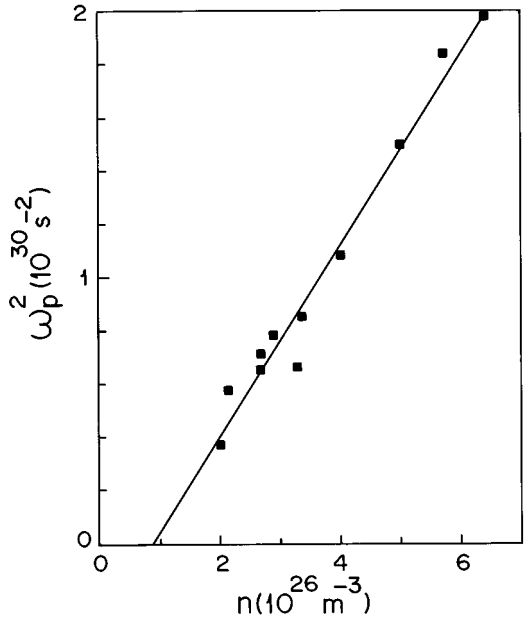

FIG. 7. Variation of the plasma resonance frequency with electron concentration. This plot yields $m_n/m_0=0.26$ and $\mu_\infty=11.8$ cm^2/Vs.

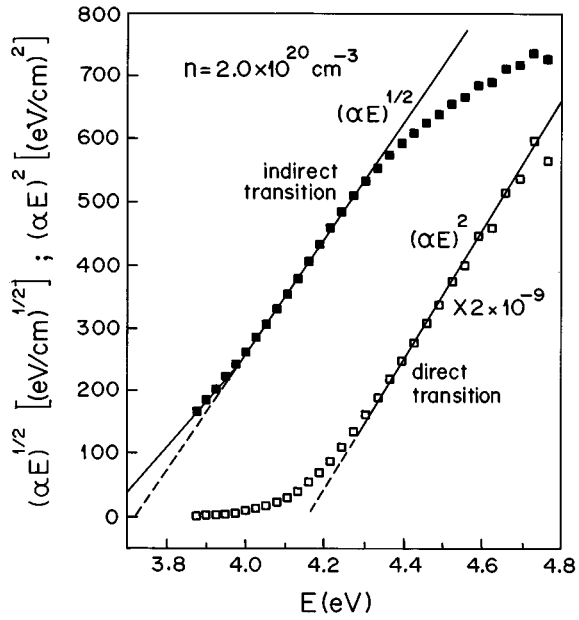

FIG. 8. Variation of $(\alpha E)^2$ and $(\alpha E)^{1/2}$ with E for a doped sample with $n=2\times10^{20}$ cm^{-3}. The values extracted for the indirect-transition energy, E_i, the direct-transition energy, E_d, and the phonon energy, E_p, are 3.68 eV, 4.16 eV and 35 meV, respectively.

This result is in contrast with that reported on antimony doped SnO_2,[9] where use of Eq. (7) (without the χ and g^2 terms) yielded m_n/m_0 values varying in the range of 0.1–0.3 for $n=0.5\times10^{20}-8\times10^{20}$ cm^{-3}.

C. Optical transitions

SnO_2 is known as a degenerate semiconductor with an energy bandgap in the range of 3.9–4.6 eV.[5] There are two possible reasons for scatter in the reported values of the energy bandgap. One is related to the method of obtaining a direct or an indirect optical transition energy from absorption coefficient data (see Sec. II B). The other is that the variation in optical transition energies measured in samples with different doping levels, the Burstein effect,[35] has been adopted mistakenly as the variation in the energy bandgap. Our experimental results will now be used to propose a model for the energy-band diagram.

Figures 8 and 9 show plots of $(\alpha E)^2$ and $(\alpha E)^{1/2}$ against E for two samples with different doping concentrations. The ranges corresponding to indirect transition and direct allowed transitions are clearly seen in both figures. The shift of the indirect-transition energy E_i and the direct-transition energy E_d to higher values with increasing n is noticeable. The energy at which the transition changes from indirect to direct also increases with doping; its value is about 4.3 eV in Fig. 8 and about 4.6 eV in Fig. 9. For samples with higher doping levels only the indirect transition was detectable in the wavelength range shown. The experimental results discussed above can be explained quantitatively by adopting the energy band diagram shown in Fig. 10.

In a degenerate semiconductor, the Fermi level lies in the conduction band. We take the energy ϵ_m below which all the energy states in conduction band are almost completely filled at room temperature to be approximately 4 kT below ϵ_{f0}, the Fermi level at 0 K. (With this choice, the probability of occupancy at ϵ_m is 98%.) The direct optical transition energy E_d is calculated as the separation between ϵ_m and the corresponding level ϵ_m' in the valence band: $E_d=(\epsilon_{f0}-\epsilon_c-4\ \mathrm{kT})+E_g+(\epsilon_{v1}-\epsilon_m')$ (see Fig. 10 for definitions). Assuming both bands are parabolic, it can be shown that $\epsilon_{v1}-\epsilon_m'=(\epsilon_m-\epsilon_c)m_n^*/m_p^*$, where $m_n^*(m_p^*)$ is the density-of-states effective mass of electrons (holes).[35] The energy difference $\epsilon_{f0}-\epsilon_c$ is readily calculated as $\epsilon_{f0}-\epsilon_c$

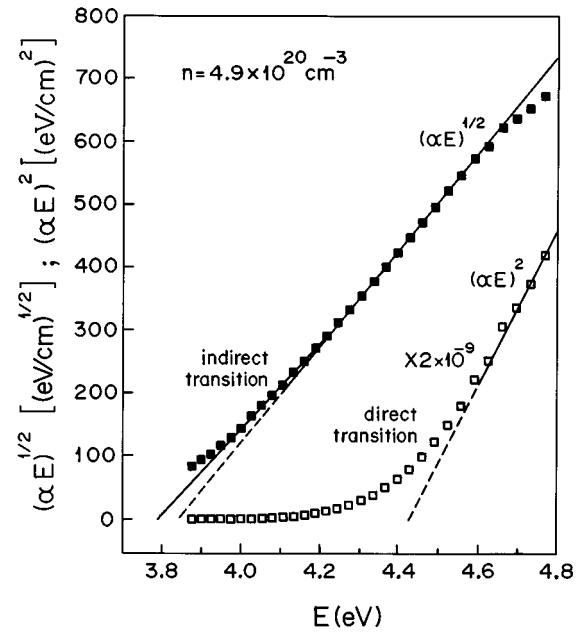

FIG. 9. $(\alpha E)^2$ and $(\alpha E)^{1/2}$ vs E plots for a doped sample with $n=4.9\times10^{20}$ cm^{-3}. The measured parameters are $E_i=3.82$ eV, $E_d=4.42$ eV, and $E_p=20$ meV.

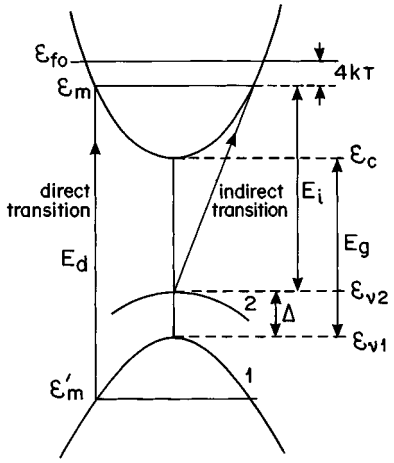

FIG. 10. The proposed energy band diagram which explains the optical transition properties in SnO_2.

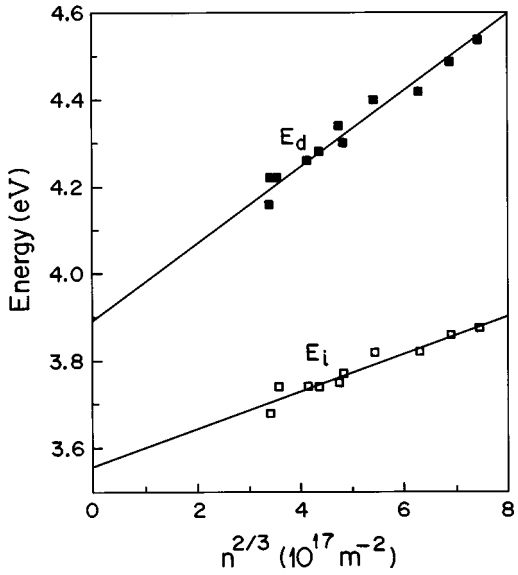

FIG. 11. The fit of the variation of the direct-transition energy (E_d) and the indirect-transition energy (E_i) with electron concentration n to Eqs. (11) and (12). The fit yields $m_p^*/m_0=0.78$, $m_n^*/m_0=0.85$, $E_g=4.11$ eV, and $\Delta=0.45$ eV.

$=\hbar^2(3\pi^2 n)^{2/3}2m_n^*$ by integrating the expression for the free electrons density of states. Thus, E_d can be written as

$$E_d=E_g-4\ \mathrm{kT}\frac{m_n^*}{m_r^*}+\frac{\hbar^2}{2m_r^*}(3\pi^2 n)^{2/3}, \tag{11}$$

where $m_r^*=m_n^*m_p^*/(m_n^*+m_p^*)$ is the reduced mass and, in terms of Planck's constant h, $\hbar=h/2\pi$.

For the indirect transition, our experimental results support the transition from another band, band 2, with an energy Δ above the former band 1 (the principal valence band). Band 2 could be a defect band. The indirect transition energy

$$E_i=\varepsilon_m-\varepsilon_{v2}=E_g-\Delta-4\ \mathrm{kT}+\frac{\hbar^2}{2m_n^*}(3\pi^2 n)^{2/3}. \tag{12}$$

Observe that both E_d and E_i are expected on the basis on Eqs. (11) and (12) to increase linearly with $n^{2/3}$.

The values of E_d and E_i were extracted from plots similar to those in Figs. 8 and 9 for samples with different doping levels. For n varying in the range of 2×10^{20} cm^{-3} to 6.4×10^{20} cm^{-3}, E_i varied from 3.68–3.88 eV and E_d varied from 4.16–4.54 eV (E_p values were in the range of 20–50 meV). Figure 11 shows the reasonably good fits of Eqs. (11) and (12) to these results. The slopes and the vertical intercepts of the two straight lines in Fig. 11 imply $E_g=4.11$ eV, $\Delta=0.45$ eV, $m_n^*/m_0=0.85$ and $m_p^*/m_0=0.78$. According to Eqs. (11) and (12), if both types of transition were taking place from the same energy band, the intercept of the E_d line with the energy axis would be slightly below that of the E_i line. This is not observed.

We conclude that SnO_2 has a direct energy bandgap of 4.11 eV and that the indirect transition involves a defect energy band, possibly associated with the nonstoichiometry of SnO_2.

IV. SUMMARY AND CONCLUSIONS

Spray-pyrolysis deposition from solution 6 (Table I), which seems to have the best composition, results in high quality films of SnO_2 with optical and electrical properties similar to those for the films deposited by the CVD technique. The sprayed films have even a higher figure of merit for photovoltaic applications. The use of HF as a source for doping is satisfactory. The undoped samples are degenerate with a resistivity in the range of 10^{-3} Ω cm. This can be lowered by a factor of ≈10 by doping. Doping with fluorine enhances the electron mobility and the film's transparency at short wavelengths. Dispersion characteristics are described well by the classical bound-electron and free-electron dispersion theories. The shift of transition energies with doping provides sufficient evidence to conclude that SnO_2 has a direct energy bandgap of 4.11 eV and a defect energy level, 0.45 eV above the valence band edge. From the optical characterization of SnO_2:F, some of the important parameters of this material, including the dispersion formula, have been determined.

ACKNOWLEDGMENT

The support of the research administration of Kuwait University under research Project No. SP048 is gratefully acknowledged.

[1] J. Britt and C. Ferekides, Appl. Phys. Lett. **62**, 2851 (1993).
[2] S. K. Das and G. C. Morris, J. Appl. Phys. **73**, 782 (1992).
[3] J. Watson, K. Ikohura, and G. S. V. Coles, Meas. Sci. Technol. **4**, 711 (1993).
[4] D. J. Yoo, J. Tamaki, S. J. Pank, N. Miura, and N. Yamazoe, J. Mater. Sci. Lett. **14**, 1391 (1995).
[5] A. L. Dawar and J. C. Joshi, J. Mater. Sci. **19**, 1 (1984).
[6] J. F. Jordan and S. P. Albright, Sol. Cells **23**, 107 (1988).
[7] C. Agashe and S. S. Major, J. Mater. Sci. Lett. **15**, 497 (1996).
[8] G. C. Morris and A. E. McElnea, Appl. Surf. Sci. **92**, 167 (1996).
[9] E. Shanthi, V. Dutta, A. Banerjee, and K. L. Chopra, J. Appl. Phys. **51**, 6243 (1980).
[10] A. L. Unaogu and C. E. Okeke, Sol. Energy Mater. **20**, 29 (1990).
[11] A. K. Abass, Solid State Commun. **61**, 507 (1987).
[12] M. T. Mohammad and W. A. Abdul-Ghafor, Phys. Status Solidi A **106**, 479 (1988).

[13] P. Cowache, D. Lincot, and J. Vedel, J. Electrochem. Soc. **136**, 1646 (1989).
[14] H. H. Afify, R. S. Momtaz, W. A. Badawy, and S. A. Nasser, J. Mater. Sci. **2**, 40 (1991).
[15] P. Grosse, F. J. Schmitte, G. Frank, and H. Kostlin, Thin Solid Films **90**, 309 (1982).
[16] *Handbook of Chemistry and Physics*, 74th ed., edited by D. R. Lide (CRC, London, 1993), pp. 4–136.
[17] A. E. Rakhshani and J. Varghese, Phys. Status Solidi A **101**, 479 (1987).
[18] A. E. Rakhshani, J. Appl. Phys. **62**, 1528 (1987).
[19] A. E. Rakhshani, J. Appl. Phys. **81**, 7988 (1997).
[20] G. A. N. Connell, R. J. Temkin, and W. Paul, Adv. Phys. **22**, 643 (1973).
[21] R. Swanepoel, J. Phys. E **16**, 1214 (1983).
[22] T. S. Moss, *Optical Properties of Semiconductors* (Butterworth, London, 1961), pp. 15–37.
[23] J. R. Dixon, in *Optical Properties of Solids*, edited by S. Nudelman and S. S. Mitra (Plenum, New York, 1969), p. 74.
[24] J. R. Dixon and H. R. Riedl, Phys. Rev **138**, A873 (1965).
[25] P. Drude, Z. Phys. **1**, 161 (1900).
[26] R. A. Smith, *Semiconductors* (Cambridge University, Cambridge, 1968), p. 189.
[27] C. R. M. Grovenor, *Microelectronic Materials* (Hilger, Bristol, 1989), p. 439.
[28] K. L. Chopra, S. Major, and D. K. Pandya, Thin Solid Films **102**, 1 (1983).
[29] D. F. Morgan and A. Wright, Br. J. Appl. Phys. **17**, 327 (1966).
[30] J. A. Marley and R. C. Dockerty, Phys. Rev. **A40**, 304 (1965).
[31] H. de Waal and F. Simonis, Thin Solid Films **77**, 253 (1981).
[32] H. L. Ma, D. H. Zhang, S. Z. Win, S. Y. Li, and Y. P. Chen, Sol. Energy Mater. Sol. Cells **40**, 371 (1996).
[33] G. Haacke, J. Appl. Phys. **47**, 4086 (1976).
[34] I. Hamberg and C. G. Granqvist, J. Appl. Phys. **60**, R123 (1986).
[35] E. Burstein, Phys. Rev. **93**, 632 (1954).